

# Transient Temperature Response of Pulsed-Laser-Induced Heating for Nanoshell-Based Hyperthermia Treatment

Changhong Liu, Chunting Chris Mi, *Senior Member, IEEE*, and Ben Q. Li

**Abstract**—This paper aims to address the transient phenomenon in pulsed-laser-induced heating for nanoshell-based hyperthermia. Within the framework of dual phase lag model, the transient temperature with the relaxation behavior involved was compared with that based on Fourier's law. The temporal variation of temperature is investigated under the irradiation of pulsed laser, as well as continuous-wave (CW) laser. A semianalytical solution of 1-D nonhomogenous dual phase lag equation in spherical coordinates is presented. The results show that the transient temperature with relaxation behavior considered is generally higher than that predicted by a classical diffusion model. The magnitude of difference depends on pulsewidth, duty cycle, and repetition rate. The maximal transient temperature is as high as 350 times the steady-state temperature in a CW case. The biological effect caused by the overheating in a short period needs to be studied further.

**Index Terms**—Diffusion model, dual phase lag model, gold nanoshell, hyperthermia, lagging behavior, pulsed laser.

## NOMENCLATURE

$a$	Inner radius [meter].
$b$	Outer radius [meter].
$A$	Coefficient in (10).
$A_s$	Coefficient caused by size effect on absorption.
$c$	Coefficient in (6).
$C_{i1}$	Coefficient in (11).
$C_{i2}$	Coefficient in (11).
$C_e$	Volumetric heat capacity of electron [joule/cubic meter/kelvin].
$C_l$	Volumetric heat capacity of lattice [joule/cubic meter/kelvin].
$C_p$	Specific heat [joule/kilogram kelvin].
$D$	Coefficient in (10).
$E$	Coefficient in (12).
$g$	Reciprocal of penetration depth [1/meter].
$G$	The phonon–electron coupling factor.
$J$	Laser fluence [joule/square meter].
$K$	Thermal conductivity [watt/meter/kelvin].

$p$	Laplacian parameter.
$q$	Heat flux [watt/square meter].
$Q$	Volumetric heating source [watt/cubic meter].
$r$	Radial coordinate [meter].
$R$	Reflectivity.
$S$	Volumetric heating source [watt/cubic meter].
$t$	Time [second].
$t_p$	Laser pulsewidth [second].
$t_M$	Laser pulse period [second].
$T$	Temperature [kelvin].
$T_0$	The initial temperature [kelvin].
$W$	Dimensionless volumetric heating source.

## Greek symbols

$\alpha$	Thermal diffusivity [square meter/second].
$\beta$	Dimensionless time.
$\beta_p$	Dimensionless laser pulsewidth.
$\beta_M$	Dimensionless laser pulse period.
$\gamma$	Coefficient.
$\delta$	Dimensionless radial coordinate.
$\varepsilon$	Ratio of $\beta_p$ over $\beta_M$ .
$\eta$	Dimensionless heat flux.
$\lambda$	Dimensionless particle radius.
$\tau_q$	Phase lag of heat flux [second].
$\tau_T$	Phase lag of temperature gradient [second].
$\Theta$	Dimensionless temperature.
$\bar{\Theta}$	Laplace transform of dimensionless temperature.

## Subscript

$i$	Layer number.
$p$	Laplace transform domain.
$q$	Heat flux.
$r$	Reference variable.
$s$	Steady state.
$T$	Temperature gradient.
1	Silica core.
2	Gold shell.
3	Tissue.

## I. INTRODUCTION

WITH the emerging techniques, it is possible to synthesize nanoparticles with a desired structure, such as cylinders, prisms, and spherical shells [1]–[3]. These particles exhibit unique optical, electromagnetic, and thermal properties at the nanoscale. Taking a gold nanoshell (silica core with thin gold coating), for instance, significant local electric field enhancement occurs due to the strong localized surface plasmon

Manuscript received October 11, 2008. First published June 2, 2009; current version published November 11, 2009. The review of this paper was arranged by Associate Editor G. Ramanath.

C. Liu and C. C. Mi are with the Department of Electrical and Computer Engineering, University of Michigan Dearborn, Dearborn, MI 48128 USA (e-mail: lchsh@umd.umich.edu; chrismi@umich.edu).

B. Q. Li is with the Department of Mechanical Engineering, University of Michigan Dearborn, Dearborn, MI 48128 USA (e-mail: benqli@umich.edu).

Color versions of one or more of the figures in this paper are available online at <http://ieeexplore.ieee.org>.

Digital Object Identifier 10.1109/TNANO.2009.2023649

resonance (LSPR). Besides, by carefully designing the core-to-shell ratio, the LSPR band can be arbitrarily tuned from visible light to the IR region [4]–[7]. These exclusive properties motivate the application of nanoshell as targeted thermal agents in cancer therapy. Because at a desired wavelength range, known as “therapeutic window,” most biological materials are transparent for the electromagnetic spectrum [8], [9]. This transparency allows a longer penetration depth [10]–[12] for laser to enter the tissue and achieve an efficient heat delivery from the skin to the targeted nanoparticles predeposited in tumor, without thermal damage to the healthy tissue.

Under appropriate irradiation, the laser-induced heat in nanoshells is gradually dissipated to the surrounding cancerous tissues, which results in 3 °C–7 °C temperature increase in the cancerous tissue. The thermal treatment between 40 °C and 44 °C, i.e., hyperthermia treatment, is believed to be cytotoxic for cells due to the change of pH environment [13], [14]. Maintaining such a condition for a certain period of time, cancerous cells finally lose their activity and die. The nanoshell-based hyperthermia (NSBH) is superior to other traditional treatments from a noninvasive and an efficient targeted viewpoint [15]. However, except a few preliminary experiments on small animals to verify the effectiveness of NSBH [16]–[18], the related theoretical research, to our best knowledge, has not been conducted systematically. This is not surprising, since the involved fundamental research ranges from plasmon physics to nonequilibrium thermodynamics to photochemistry, and so on. It is no doubt an interdisciplinary subject.

Since the primary concern in all types of cancer therapies, without exception, is to minimize damage to the healthy parts of the body, it is of vital importance to predict the temperature rise during thermal therapy. It has been reported that protein denaturation occurs at a temperature of 50 °C for most biotissues [19], and cells die at a temperature of about 70 °C in a few seconds [20]. Even though the steady-state temperature in NSBH can be controlled under 44 °C, it does not mean the maximum temperature is 44 °C. Due to the large thermal relaxation time of the tissue, the fast transient temperature may be far beyond our expectations. Although exact data about cellular survival under high temperature and short duration remain unknown, it is not inconceivable that with the temperature greatly elevated, the tolerance time of healthy cells decreases. In view of the aforementioned fact, as part of a fundamental study, this paper aims to address the transient phenomenon of heat conduction in pulsed-laser-induced NSBH.

In most of engineering applications, heat conduction can be accurately described by the classical Fourier’s law, which assumes that any thermal disturbance causes an instantaneous response throughout the object, or equivalently, the propagation speed of heat is infinite. However, this assumption is questionable in case of problems involving a micro/nano spatial/temporal scale. This has been proved in the literature [21]–[24]. Within the macroscopic framework, a temperature field is assumed not only continuum, but also holding thermal equilibrium at every location. When the length scale is comparable to or smaller than the mean free path of a material, there are no sufficient energy carriers in the interested direction. Therefore, the temperature

field is no longer continuous. Once the concept of temperature gradient fails, the classical Fourier’s law is also questionable, and so is the associated diffusion equation. A similar situation exists in the response time for temperature. The macroscopic heat equation assumes that temperature gradient follows simultaneously with heat flux vector. In fact, any physical process needs a finite time to take place. As a result, once the response time of primary concern is in the same order of the mean free time, the lagging behavior caused by phonon–electron interaction in metal films or phonon scattering in dielectric media must be taken into account. In NSBH, the interaction of short pulsed laser with a nanoparticle with a shell thickness of 2–10 nm determines that both microspatial and microtemporal issues are involved. Therefore, the microscopic heat conduction model should be used instead of the macroscopic model. So far, to our best knowledge, only a few publications studied the heat transfer mechanism of NSBH from the microscopic prospective.

To account for the microscopic heating problems, some modified heat conduction models were proposed in the previous work. Cattaneo [25] and Vernotte [26] proposed the macroscopic thermal wave model (CV wave model) to consider a finite speed of thermal propagation. The limitation of the CV model is that it only contributes to a microscopic response in time without consideration of the microstructured effect. As an alternative, Pan presented a numerical simulation from a molecular dynamic viewpoint to consider the microstructured effect on temperature [27]. The two-step model is another frequently employed model in processing the interaction of pulsed laser with a metal film. It was pioneered by Kaganov *et al.* [28] and Anisimov *et al.* [29], and advanced by Qiu and Tien [30]. The two-step model captures the fast transient heating behavior as two separate stages, i.e., the radiation energy deposited on electrons, then energy exchange between electrons and the lattice. The hyperbolic two-step model is derived from quantum mechanical and statistical basis. Therefore, it modified the phenomenological nature of the CV model. Compared to the two-step model whose emphasis is on the metal film, the phonon scattering model (pure phonon scattering model), proposed by Guyer and Krumhansl [31], puts major emphasis on heat transport by phonon scattering. So, it is generally used in evaluating the thermal behavior of a dielectric solid. To describe the microscopic heat phenomenon both in time and space, both for metal and dielectric, Tzou developed a dual phase lag (DPL) model [32], in which two lumped relaxation time parameters were introduced to depict the transient thermal phenomenon on a microscopic scale. The details of the DPL model will be explained in the next section.

The work in this paper is considered a continuation of the electromagnetic analysis of laser–nanoshell interaction published earlier by the authors [33]. As an initial stage of exploration, this paper focuses on the transient temperature behavior of a single nanoshell and its adjacent tissue under the exposure of a pulsed laser, as shown in Fig. 1. For this purpose, we put little emphasis on the propagation of the laser through the skin and the tissue it passes through, i.e., the laser has been assumed to have successfully arrived at the tumor region. In addition, as a first attempt, it is assumed that the surface of gold shell makes

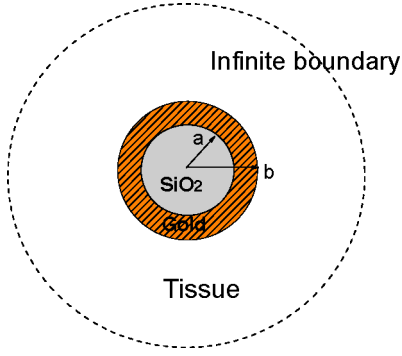


Fig. 1. Schematic diagram for laser-induced heating. An isolated gold nanoshell, with outer radius  $b = 30$  nm and inner radius  $a = 27$  nm, is embedded in infinite tissue-like media and irradiated by a single-pulse laser. The heat generation inside the shell is assumed to be uniformly distributed. Thus, the mathematical model reduces to a transient 1-D nonhomogenous heat conduction problem in the spherical coordinate.

perfect contact with both silica core and the host tissue. However, it should be stated that in real applications, the nanoshell surface is not smooth due to the chemical synthesis process. Moreover, the outer nanoshell surface is modified with thiolated polyethylene glycol (PEG) to provide steric stabilization as well as eliminate nonspecific protein adsorption. Therefore, the contact thermal resistance caused by the rough surface and the biomatter modification remain a challenging issue so far.

## II. MODEL DESCRIPTION

### A. DPL Model

The original DPL concept can be mathematically expressed as [31]

$$\vec{q}(\vec{r}, t + \tau_q) = -k\nabla T(\vec{r}, t + \tau_T) \quad (1)$$

where  $t$  is the time instant at which conservation of energy is imposed, and  $\tau_q$  is the phase lag of the heat flux vector. At time instant  $t + \tau_q$ , heat flows through the material volume.  $\tau_T$  is the phase lag of the temperature gradient. At time instant  $t + \tau_T$ , the temperature gradient is established across a material volume.

Tang *et al.* interpreted the physical explanation of these two parameters from the microscale sense [34]. For dielectric crystals, by comparing the DPL model with the pure phonon field model [30], it can be found that  $\tau_q$  is the relaxation time for the momentum-nonconserving process and  $\tau_T$  is the relaxation time for the normal process conserving the momentum in the phonon system. For metals, by comparing with the micro two-step model [30], it is found that  $\tau_T$  captures the time delay due to the microstructural interaction effect, i.e., the finite time required for phonon–electron interaction to take place, and  $\tau_q$  captures the time delay due to the fast transient effect of thermal inertia. The two parameters,  $\tau_T$  and  $\tau_q$ , account for the time required by both heat flux and temperature gradient to gradually respond to thermal disturbances, such as an imposed temperature difference or heating.

The first-order expansion of (1) with respect to  $t$  is

$$\vec{q}(\vec{r}, t) + \tau_q \frac{\partial \vec{q}(\vec{r}, t)}{\partial t} \approx -k \left\{ \nabla T(\vec{r}, t) + \tau_T \frac{\partial}{\partial t} [\nabla T(\vec{r}, t)] \right\}. \quad (2)$$

Taking the divergence of (2) and substituting  $\nabla \cdot \vec{q}$  to the energy equation established at a general time  $t$

$$-\nabla \cdot \vec{q}(\vec{r}, t) + S(\vec{r}, t) = C_p \frac{\partial T(\vec{r}, t)}{\partial t}. \quad (3)$$

The  $T$  representation of the DPL model is

$$\nabla^2 T + \tau_T \frac{\partial}{\partial t} \nabla^2 T + \frac{1}{K} \left[ S + \tau_q \frac{\partial S}{\partial t} \right] = \frac{1}{\alpha} \frac{\partial T}{\partial t} + \frac{\tau_q}{\alpha} \frac{\partial^2 T}{\partial t^2} \quad (4)$$

subject to the following boundary conditions:

$$\begin{aligned} T_1(a, t) &= T_2(a, t) \\ q_1(a, t) &= q_2(a, t) \\ T_2(b, t) &= T_3(b, t) \\ q_2(b, t) &= q_3(b, t) \\ \frac{\partial T_1(0, t)}{\partial r} &= 0 \\ T_3(\infty, t) &= T_0 \end{aligned} \quad (5)$$

and the initial condition

$$T(r, 0) = T_0.$$

It is noted that when  $\tau_q = \tau_T$ , (1) reduces to Fourier's law, and the DPL model in (4) becomes the diffusion equation. If  $\tau_T = 0$ , then (4) becomes the CV wave model originated by Cattaneo and Vernotte.

### B. Intensity of Pulsed Laser

In (4), variable  $S$  represents the intensity of a laser beam, i.e., the volumetric heat source in the analytical modeling. The energy distribution of a single pulsed laser is assumed exponentially decaying with laser propagation in space and with a Gaussian profile in time. The pulsed volumetric heating of a single pulse is, thus, expressed as [32]

$$\vec{S}(\vec{r}, t) = 0.94Jg \left( \frac{1-R}{t_p} \right) e^{-g \cdot |b-r| - \frac{c|t-2t_p|}{t_p}} \cdot A_s \quad (6)$$

where  $A_s$  is size effect on laser absorption. In the case of system size being smaller than the mean free path of metal electrons, the collisions between electrons and matter boundaries need to be taken into account. As a result, the optical absorption performance needs to be modified as well [35]. Fig. 2 illustrates the absorption efficiency with the size effect involved, where we obtain  $A_s = 0.25$  at the LSPR wavelength.

The volumetric heat source from the repetitive laser pulses can be arranged by a sequence of single pulses

$$S(r, t) = S_0 e^{-g(b-r)} \sum_{i=0}^{N-1} g_i(t) \quad (7)$$

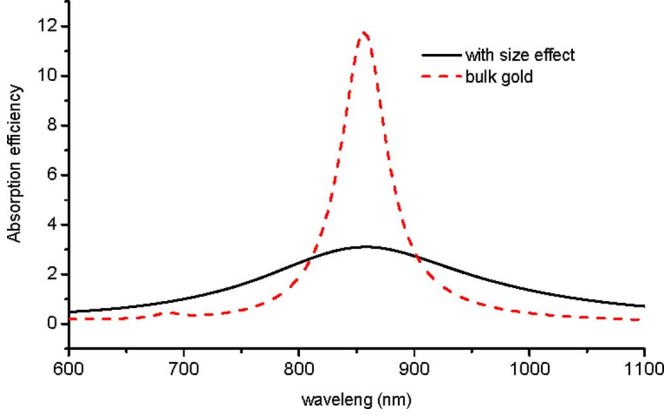


Fig. 2. Size effect on laser absorption. The resonance peak for a 27/30 nm gold nanoshell with size effect involved is only 0.25 as much as that of bulk gold at the LSPR wavelength. The refractive index of bulk gold is given in [36], and in case of 3 nm shell thickness, it is modified according to [35].

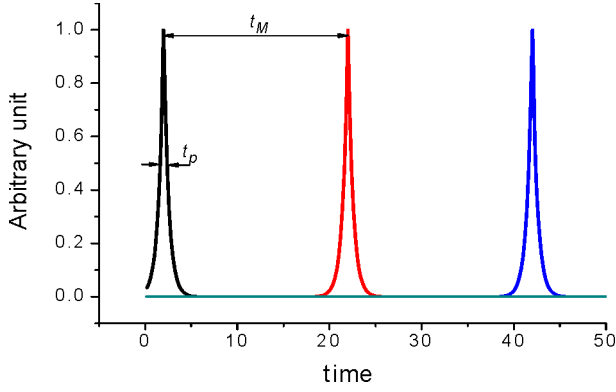


Fig. 3. Construction of a pulsed laser train.

where  $N$  is the total number of laser pulses

$$g_i(t) = e^{-\frac{c|t-it_M-2t_p|}{t_p}} \{u(t-it_M) - u(t-(i+1)t_M)\}$$

$$S_0 = 0.94Jg\left(\frac{1-R}{t_p}\right) \cdot A_s$$

and  $u(t)$  the unit step function:

$$u(t) = \begin{cases} 1 & t > 0 \\ 0 & t < 0 \end{cases}$$

The temporal profile given by (7) is shown in Fig. 3.

### C. Semianalytical Solution

By introducing the following dimensionless variables

$$\Theta = \frac{T - T_r}{T_r} \quad \beta = \frac{t}{\tau_{qr}} \quad \delta = \frac{r}{\sqrt{\alpha_r \tau_{qr}}} \quad \alpha_{ri} = \frac{\alpha_i}{\alpha_r}$$

$$K_{ri} = \frac{K_i}{K_r} \quad \tau_{Tri} = \frac{\tau_{Ti}}{\tau_{qr}} \quad \tau_{qri} = \frac{\tau_{qi}}{\tau_{qr}} \quad W = \frac{S}{k_r T_r / \alpha_r \tau_{qr}}$$

Equation (4) in spherical coordinates can be written as

$$\left(\frac{\partial^2 \Theta}{\partial \delta^2} + \frac{2}{\delta} \frac{\partial \Theta}{\partial \delta}\right) + \tau_{Tri} \frac{\partial}{\partial \beta} \left(\frac{\partial^2 \Theta}{\partial \delta^2} + \frac{2}{\delta} \frac{\partial \Theta}{\partial \delta}\right) + \frac{1}{K_{ri}} \left(W + \tau_{qri} \frac{\partial W}{\partial \beta}\right) = \frac{1}{\alpha_{ri}} \frac{\partial \Theta}{\partial \beta} + \frac{\tau_{qri}}{\alpha_{ri}} \frac{\partial^2 \Theta}{\partial \delta^2}. \quad (8)$$

Applying the Laplace transform to (8) yields

$$\left(\frac{\partial^2 \bar{\Theta}}{\partial \delta^2} + \frac{2}{\delta} \frac{\partial \bar{\Theta}}{\partial \delta}\right) - \frac{(1 + \tau_{qri} p) p}{\alpha_{ri} (1 + \tau_{Tri} p)} \bar{\Theta} + \frac{1 + \tau_{qri} p}{K_{ri} (1 + \tau_{Tri} p)} \bar{W} - \frac{\tau_{qri}}{K_{ri} (1 + \tau_{qri} p)} \bar{W}(\delta, 0) = 0 \quad (9)$$

where

$$\bar{W}(\delta, 0) = W_0 e^{-g_0 \delta - 2c} \quad W_0 = \frac{S_0}{k_r T_r / \alpha_r \tau_{qr}}$$

$$g_0 = g \sqrt{\alpha_r \tau_{qr}} \quad \bar{W}(\delta, p) = \frac{S(\delta, p)}{k_r T_r / \alpha_r \tau_{qr}}$$

$$S(\delta, p) = L\{S(\delta, \beta)\} = W_0 e^{-g_0 \delta} L\left\{\sum_{i=0}^{N-1} g_i(\beta)\right\}$$

$$= W_0 e^{-g_0 \delta} \sum_{i=0}^{N-1} g_i(p)$$

$$g_i(\beta) = e^{-\frac{a|\beta - i\beta_M - 2\beta_p|}{\beta_p}} \{u(\beta - i\beta_M) - u(\beta - (i+1)\beta_M)\},$$

$$\beta_p = \frac{t_p}{\tau_{qr}}, \quad \beta_M = \frac{t_M}{\tau_{qr}}$$

$$g_i(p) = L(g_i(\beta)) = \beta_p \left[ \frac{e^{-p(i\beta_M + 2\beta_p)} - e^{-2a - ip\varepsilon}}{a - p\beta_p} + \frac{e^{-p(i\beta_M + 2\beta_p)} - e^{a(2-\varepsilon) - p(i+1)\beta_M}}{a + p\beta_p} \right]$$

with  $\varepsilon = \frac{\beta_p}{\beta_M}$ .

Introducing  $\bar{\Theta} = \bar{U}/\delta$ , after some algebraic manipulations, (9) becomes

$$\frac{\partial^2 \bar{U}}{\partial \delta^2} - A_i \bar{U} + D_i \cdot \delta = 0 \quad (10)$$

where

$$A_i = \frac{(1 + \tau_{qri} p) p}{\alpha_{ri} (1 + \tau_{Tri} p)} \quad D_i = \frac{(1 + \tau_{qri} p) \bar{W} - \tau_{qri} W(\delta, 0)}{K_{ri} (1 + \tau_{Tri} p)}$$

with subscript  $i$  from 1 to 3 representing the silica core, gold shell, and tissue, respectively. Since variable  $D$  is the source term, only  $D_2$  exists,  $D_1 = D_3 = 0$ . Equation (8) is a differential equation written in the dimensionless variables in the Laplacian transform domain. It is straightforward to obtain the general solution of  $\bar{\Theta}$  for (10) in the following form:

$$\bar{\Theta}_i(\delta; p) = \frac{\bar{U}_i(\delta; p)}{\delta} = \frac{D_i}{A_i} + \frac{C_{i1} e^{\sqrt{A_i} \delta} + C_{i2} e^{-\sqrt{A_i} \delta}}{\delta}. \quad (11)$$

The six coefficients  $C_{i1}, C_{i2}, i = 1, 2, 3$  can be determined by the boundary conditions described in (5). By introducing a

nondimensional heat flux variable  $\eta = \frac{q}{k_r T_r / \sqrt{\alpha_r \tau_{qr}}}$ , the boundary conditions in (5) are rewritten as follows:

$$\begin{cases} \bar{\Theta}_1 = \bar{\Theta}_{2a}, & \text{at } r = a \\ \bar{\eta}_1 = \bar{\eta}_{2a}, & \text{at } r = a \\ \bar{\Theta}_{2b} = \bar{\Theta}_3, & \text{at } r = b \\ \bar{\eta}_{2b} = \bar{\eta}_3, & \text{at } r = b \\ \bar{\eta}_1 = 0, & \text{at } r = 0 \\ \bar{\Theta}_3 = 0, & \text{at } r = \infty. \end{cases} \quad (12)$$

In the lagging behavior model

$$q(r, t) \neq -k\nabla T(r, t)$$

instead

$$q(r, t + \tau_q) = -k\nabla T(r, t + \tau_T).$$

The first-order expansion is

$$q(r, t) + \tau_q \frac{\partial q(r, t)}{\partial t} \approx -k \left[ \nabla T(r, t) + \tau_T \frac{\partial}{\partial t} \nabla T(r, t) \right]. \quad (13)$$

Applying dimensionless analysis

$$\eta(\delta, \beta) + \tau_{qri} \frac{\partial \eta(\delta, \beta)}{\partial \beta} \approx -k_{ri} \left[ \frac{\partial \Theta}{\partial \delta} + \tau_{Tri} \frac{\partial^2 \Theta}{\partial \delta^2} \right].$$

Taking Laplace transformation with respect to  $\beta$

$$\bar{\eta}(\delta; p) \approx -E_i \cdot \frac{\partial \bar{\Theta}}{\partial \delta} \quad (14)$$

where  $E_i = \frac{K_{ri}(1 + \tau_{Tri} p)}{1 + \tau_{qri} p}$ .

Combining (10) and (14), one can get

$$\bar{\eta}(\delta; p) \approx -E_i \cdot \frac{\partial \bar{\Theta}}{\partial \delta} - E_i \left[ -\frac{C_{i1} e^{\sqrt{A_i} \delta} + C_{i2} e^{-\sqrt{A_i} \delta}}{\delta^2} + \frac{C_{i1} \sqrt{A_i} e^{\sqrt{A_i} \delta} - C_{i2} \sqrt{A_i} e^{-\sqrt{A_i} \delta}}{\delta} \right]. \quad (15)$$

The six coefficients in (11) can be determined from (12) and the solution of  $\bar{\Theta}$  in the Laplace transform domain is also obtained. The Laplacian inversion of (14) is computed using the Riemann-sum approximation given by [13]

$$\Theta(\delta, \beta) = \frac{e^{\gamma \beta}}{\beta} \left[ \frac{1}{2} \bar{\Theta}(\delta, \gamma) + \text{Re} \sum_{n=1}^{\infty} \bar{\Theta} \left( \delta, p = \gamma + j \frac{n\pi}{\beta} \right) (-1)^n \right] \quad (16)$$

which is the inverse Laplace transform of  $\bar{\Theta}(\delta, p)$ . For faster convergence, numerical experiments have shown that a value satisfying  $\gamma = 4.7$  gives satisfactory results in most cases [32].

#### D. Phase Lag Parameters $\tau_T$ and $\tau_q$

Since both microstructured and microtemporal effects have been lumped into the resultant delayed response in time, the constant values of  $\tau_T$  and  $\tau_q$  are crucial for the description

TABLE I  
THERMAL PROPERTIES OF GOLD, TISSUE, AND SILICA

	$k$ (W/m.K)	$\alpha$ (m <sup>2</sup> /s)	$\tau_T$ (s)	$\tau_q$ (s)
gold	315	$1.18 \times 10^{-4}$	$89.286 \times 10^{-12}$ [32]	$0.7438 \times 10^{-12}$ [32]
tissue	0.80	$1.40 \times 10^{-7}$	0.043 [39]	16 [39]
silica	1.0	$9 \times 10^{-7}$	$10 \times 10^{-12}$ [37]	$5 \times 10^{-12}$ [37]

of the heat transport in microscopic scale. Physically,  $\tau_T$  and  $\tau_q$  are regarded as the macroscopic parameters of a series of microscopic physical processes, i.e., electron–electron interaction, phonon–electron interaction, and phonon scattering, but not simply summation. The determination of  $\tau_T$  and  $\tau_q$ , either theoretically or experimentally, remains a problem. Relatively speaking, the characteristic time of metal is easy to obtain due to the regular arrangement of crystal. For a metal film, by comparing the DPL model with the hyperbolic two-step model [30], Tzou [32] developed the direct relationship of the two characteristic time constants with the microscopic thermal properties, which is

$$\alpha = \frac{K}{C_e + C_l} \quad \tau_T = \frac{C_l}{G} \quad \tau_q = \frac{1}{G} \left[ \frac{1}{C_e} + \frac{1}{C_l} \right]^{-1} \quad (17)$$

where  $G$  is a function of electron mass, electron gas density per unit volume, the Planck constant, the Boltzmann constant, and the Debye temperature. On this basis, the value of  $\tau_T$  and  $\tau_q$  of a gold film is given in Table I.

In this paper, to determine  $\tau_T$  and  $\tau_q$  for silica, we have adopted the parameters provided by Tzou [37].

To date, the characteristic time of biotissue is still in dispute. No unified conclusion has been reached due to the complexity of tissue components. Vedavaz *et al.* [38] used the expression  $\tau_{\text{phonon}} = 3\alpha/v^2$  to estimate the value of relaxation time of biological tissue, which gives 1–100 s at room temperature. Mitra *et al.* [39] performed four experiments with different boundary conditions and found that  $\tau_q$  in the processed meat was about 16 s and  $\tau_T$  was about 0.043 s. Kaminski [40] estimated that  $\tau_q$  is in the range of 20–30 s. Banerjee *et al.* [41] used relaxation time of 5 s to carry out the theoretical non-Fourier hyperbolic heat analysis and found it is closer to the experiment results than that with the parabolic Fourier heat conduction. However, heat transfer models [42]–[44] suggest heat is transferred within 100–300 ps from nanoparticles into the nearby water shell. The exact parameter difference between water and biotissue needs further investigation. In this paper, we use  $\tau_T = 0.043$  s and  $\tau_q = 16$  s [39], as indicated in Table I.

### III. RESULTS AND DISCUSSIONS

This section has two parts. One is about the temperature response of a single laser pulse excitation. The emphasis is on the effects of thermal lagging behavior of silica core and biological tissue on temporal variation of temperature and the effect of pulsewidth. The other is about the temperature variation with a pulsed-laser-induced excitation, aiming at the comparison of temperature response of continuous-wave (CW) laser and pulsed laser by means of the DPL model and the diffusion model.

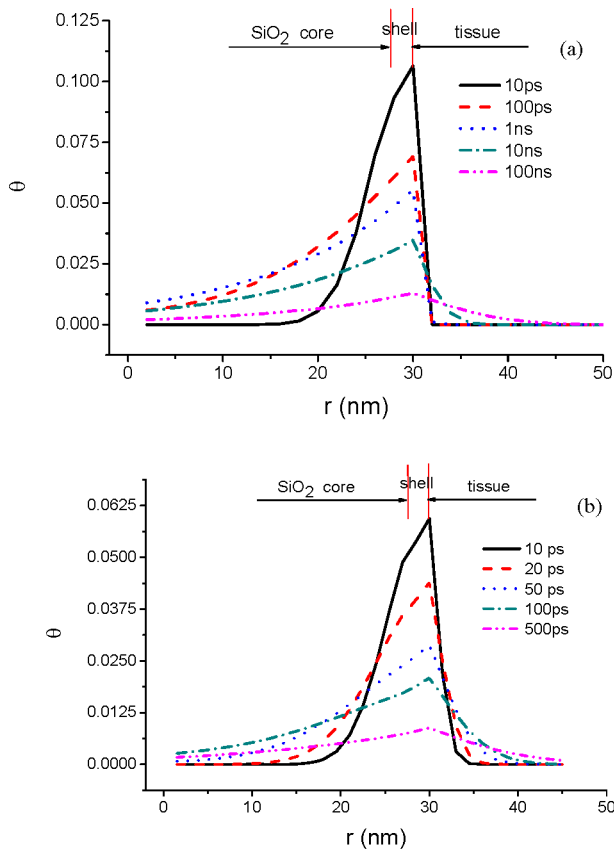


Fig. 4. Transient temperature distribution near a single nanoshell, with inner radius of 27 nm and shell thickness of 3 nm. The duration of the laser pulse is 1 ps. (a) Temperature obtained from the DPL model. (b) Temperature obtained from the classical diffusion model.

#### A. Single Laser Pulse Interacting With Single Nanoshell

1) *Effect of Tissue on Transient Temperature:* As a study case, the energy from a single laser pulse with duration  $t_p = 1$  ps was considered. The semi-DPL model and the classical diffusion model were employed, respectively, to capture the temperature history at different time instants. In the former, the characteristic time ( $\tau_T$  and  $\tau_q$ ) of gold and the tissue were assigned according to Table I, and  $\tau_T$  and  $\tau_q$  of silica were set zero. The purpose is to separately exhibit the effect of different materials on the transient temperature. Fig. 4 shows that the maximal temperature occurs at the interface of the nanoparticle and tissue.

By comparing the temperature of the DPL model shown in Fig. 4(a) with the temperature of the diffusion model shown in Fig. 4(b), we can find an important phenomenon: at instant  $t = 10$  ps,  $\theta$  of the DPL model is higher than 0.1, while  $\theta$  of the diffusion model is lower than 0.0625. The same situation occurs at instant  $t = 100$  ps. This implies that the effect of thermal relaxation is caused by the tissue. In the diffusion model, thermal disturbance is assumed to cause an instantaneous response without any delay. Therefore, heat inside the shell is transferred to its adjacent tissue as soon as heat generates. In the semi-DPL model, however, tissue needs time to respond to the sudden thermal load. As a result, heat accumulates inside

the particle until the tissue begins to respond, which causes a higher temperature rise inside the particle in the DPL model. We tried a series of characteristic times of a tissue-like material, and found that the bigger the difference of  $\tau_q - \tau_T$  in the tissue, the higher the overshooting of the temperature inside the particle due to the long-time heat accumulation without dissipation.

2) *Effect of Silica Core on Transient Temperature:* In this case, the transient temperatures with the semi-DPL model and DPL model were compared. In the semi-DPL model, the silica core is assumed diffusive, i.e.,  $\tau_{T1} = \tau_{q1} = 0$ , while, in the pure DPL model,  $\tau_{T1} = 10$  ps and  $\tau_{q1} = 5$  ps. We arbitrarily select pulsewidth with 10 ps to examine the influence of the lagging behavior of the silica core to the transient temperature. Fig. 5 depicts four time instants,  $t = 1$  ps,  $t = 10$  ps,  $t = 20$  ps, and  $t = 500$  ps. We can conclude that in the pulsewidth, the temperature increases with time; then, the temperature gradually drops. In addition, we found an inverse trend, as shown in Fig. 3, where the heat flux vector of the tissue lags behind the temperature gradient. The equivalent relaxation time of the tissue  $\tau_q - \tau_T$  is positive, which contributes to an overshooting in the temperature profile. While in Fig. 5, the heat flux vector of silica precedes the temperature gradient. The equivalent relaxation time  $\tau_q - \tau_T$  is negative, which represents the case of overdiffusion. However, given the fact that  $\tau_q$  is comparable to  $\tau_T$ , the phenomenon of overdiffusion is not very obvious.

3) *Pulsewidth Effect on Transient Temperature:* The purpose of this section is to investigate the temperature difference predicted by the DPL model and the diffusion model under varying pulsewidths. We use a temperature ratio with respect to the maximal temperature of the DPL model to evaluate the relative temperature difference caused by different models. From Fig. 6(a) to (d), the pulsewidth is assigned 1, 10, 100, and 1000 ps, respectively. In Fig. 6(a), if the maximal temperature of DPL is 1, the corresponding temperature of the diffusion model goes to 0.83. With pulsewidth increasing, if we still use the maximal  $\theta$  as a reference,  $\theta$  of diffusion case goes to 0.52, 0.11, and 0.02, respectively. This means that the wider the pulsewidth, the bigger the temperature difference between the DPL model and the diffusion model. For instance, at  $t_p = 1$  ps, the maximal  $\theta$  described by the DPL model is about 1.2 times that of the diffusion model. However, at  $t_p = 1000$  ps, the maximal  $\theta$  of the DPL model becomes 50 times that of the classical heat conduction model. This means that for a temperature rise of 1 °C predicted by the diffusion model, the actual temperature rise will be 50 °C if we consider the relaxation behavior contributed by the biological tissue. We can further conclude that the temperature will keep increasing if the pulsewidth is even longer until it becomes bigger than  $\tau_q - \tau_T$  of the tissue, since the tissue begins to dissipate heat at this instant.

Although we are not sure to what extent such high temperature affects biotissue in short duration, we have to take appropriate measures to avoid the possible overheat damage to the tissue. These measures may include appropriate concentration of particles, reasonable pulsewidth, and intensity, etc. This will be our further direction of research on NSBH.

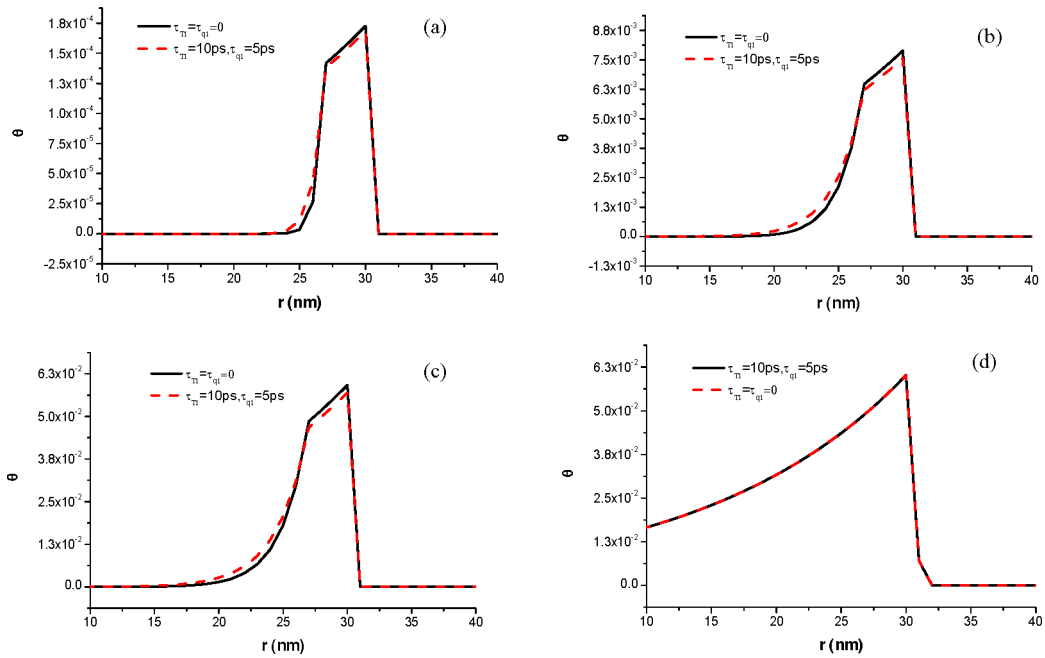


Fig. 5. Temperature distribution at various time instants. The pulsewidth is 10 ps. The solid lines represent the results from the semi-DPL model and the dashed lines denote results from the DPL model. (a)  $t = 1$  ps. (b)  $t = 10$  ps. (c)  $t = 20$  ps. (d)  $t = 500$  ps.

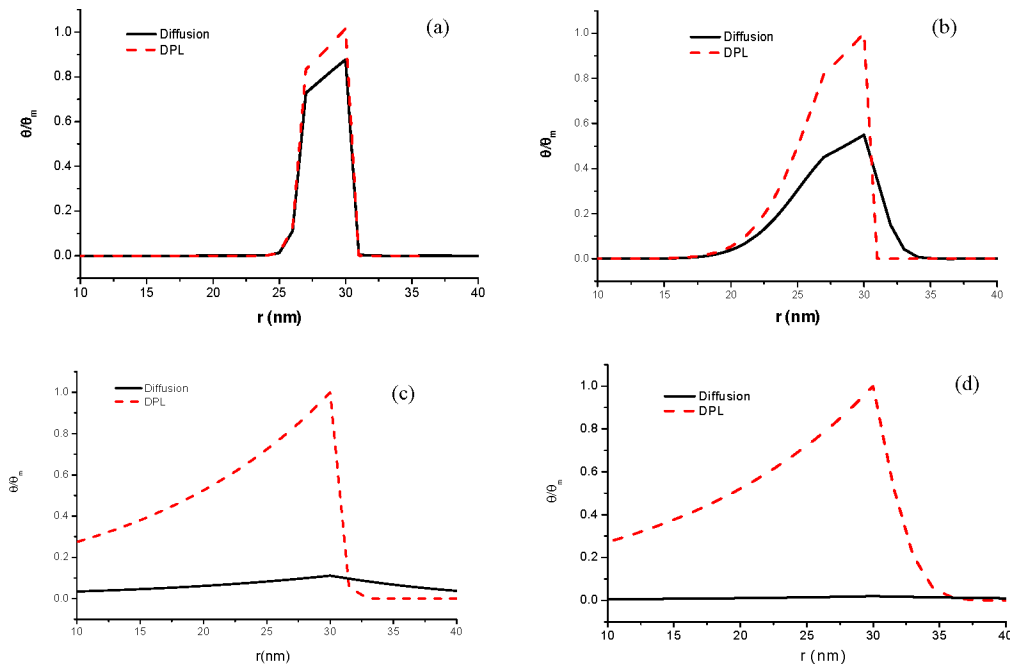


Fig. 6. Duration effect on transient temperature with the DPL model. (a)  $t_p = 1$  ps. (b)  $t_p = 10$  ps. (c)  $t_p = 100$  ps. (d)  $t_p = 1000$  ps.

### B. Pulsed Laser Interacting With a Single Nanoshell

1) *Temperature History Versus Varying Duty Cycle:* Fig. 7(a) shows the temporal variation of the interface temperature between the shell and tissue ( $r = 30$  nm) with the same pulsewidth (1 ps), but different duty cycles of laser pulses. The three curves represent duty cycles of 10%, 5%, and 2.5%, respectively. The same pulsewidth implies the same magnitude of temperature rise in the early heating period of each laser pulse. As time elapses,

the laser energy is exponentially weakened, and the temperature tends to decrease. Obviously, the time-average temperature depends on duty cycle, as well as repetition rate. A larger number of pulses increases the total internal energy absorbed by the nanoshell, which, in turn, increases the temperature rise of the particle and the adjacent tissue.

Fig. 7(b) shows the temporal variation of the interface temperature under another situation, i.e., the same pulsewidth, but a different duty cycle. However, the time-average power is

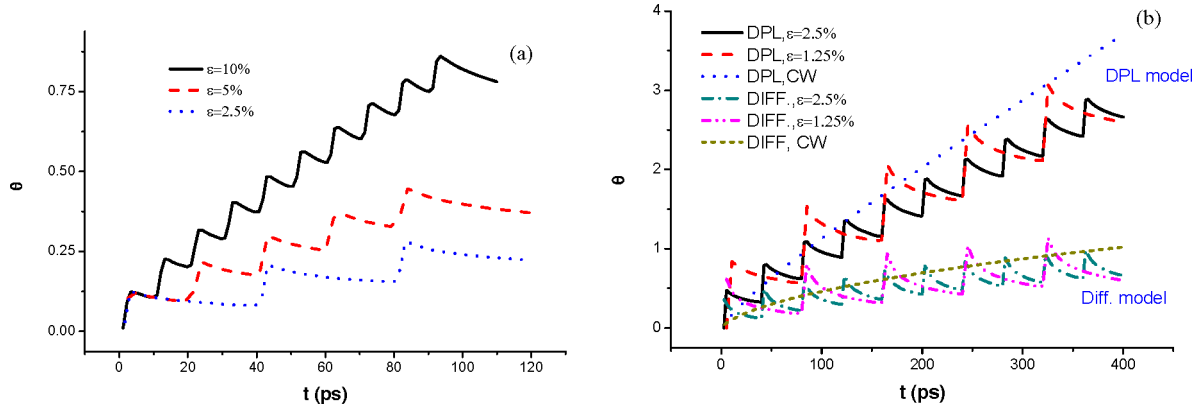


Fig. 7. Temperature response with repetitive pulsed laser. (a) Duty cycle effect on temperature response. (b) Temporal variation of the interface temperature under the same pulsewidth, but with a different duty cycle.

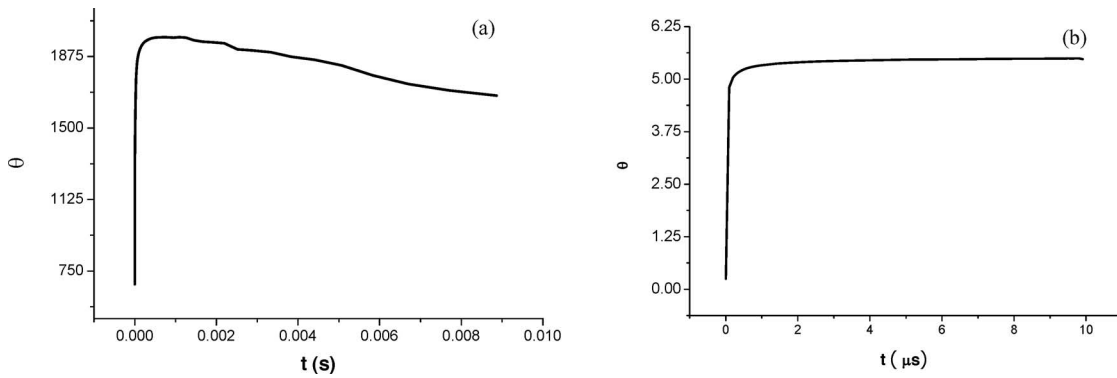


Fig. 8. Temporal variation of interface temperature with CW excitation in long time scale. (a) DPL model. (b) Diffusion model.

constant in the interested time period, e.g., 100 ps. To achieve this, the intensity of the pulse laser needs to be increased to maintain identical energy. By assuming  $\varepsilon < 50\%$ , the expression of average energy can be simply expressed as

$$\begin{aligned}
 S_{\text{av}}(r, t) &= \frac{1}{t_D} \int_0^{t_D} S(r, t) dt = \frac{S_0 e^{-gr}}{t_D} \int_0^{t_D} e^{-\frac{c|t-2t_p|}{t_p}} dt \\
 &= \frac{S_0 e^{-gr}}{t_D} \left\{ \int_0^{2t_p} e^{-\frac{c(2t_p-t)}{t_p}} dt + \int_{2t_p}^{t_D} e^{-\frac{c(t-2t_p)}{t_p}} dt \right\} \\
 &= \frac{S_0 e^{-gr}}{t_D} \frac{t_p}{c} \left[ 2 - e^{-2c} - e^{c(2-\varepsilon)} \right]. \quad (18)
 \end{aligned}$$

The upper three curves in Fig. 7(b) are simulated by the DPL model, and the lower three curves by the diffusion model. By comparing the pulse condition with the CW condition for the DPL model with the diffusion model, it can be seen that although the average power and pulsewidth are the same, a relatively high transient temperature rise can be obtained by concentrating all the laser energy into a very short period of duration. But the transient temperature with pulse excitation is not always higher than that with CW laser. It depends on both pulsewidth and duty cycle. Besides, the temperature with pulse laser excitation in the DPL simulation tends to be smaller than the CW result. However, in the diffusion model the tendency is just the opposite. In addition, the temperature with relaxation behavior considera-

tion is generally higher than those with diffusion consideration. Take the CW case, for instance, at  $t = 400$  ps, the dimensionless temperature of the DPL model is almost 3.5 times the diffusive result, and the difference tends to be enlarged with time elapses. Naturally, we need to investigate what happens with time.

In Fig. 8, the temporal variation of the interface temperature with CW excitation in the long time scale is calculated by the DPL model and the diffusion model, respectively. Fig. 8(b) indicates that during the period of phase lag of the tissue, the maximal temperature is as high as 2000, and after that heat begins to dissipate toward the tissue, followed by a gradual temperature decrease. It can be confirmed that with time elapses, the effect caused by the lagging behavior, mainly contributed by the tissue, will become weaker and weaker. If the time is long enough, the temporal profile of the temperature should coincide with that of the diffusion model, which is shown in Fig. 7(b). The steady-state temperature is around 5.6. Obviously, the maximal transient temperature reaches as high as 350 times the steady-state value. Thus, if the steady-state temperature rises by  $1^\circ\text{C}$ , the temperature at one time will reach  $350^\circ\text{C}$  at the interface.

It must be noted that it is the temperature comparison between the DPL model and the diffusion model, not the absolute value of temperature, that makes sense in this paper. The temperature field in NSPH is contributed by hundreds of thousands of nanoparticles and the temperature of a single nanoparticle does not represent the overall or average temperature. Consequently,

the intensity of laser in this paper is arbitrarily assigned. However, it does not affect the analysis of the transient heat transport phenomenon.

#### IV. CONCLUSION

Within the framework of the DPL model, the transient heat transfer process was studied for gold NSBH treatments. The influence of the thermal lagging behavior of silica core and biological tissue on temporal variation of temperature was discussed separately in terms of two lumped phase lag parameters,  $\tau_T$  and  $\tau_q$ . Analytical results indicate that a bigger  $\tau_q$  of the tissue has a larger effect on the overall temperature of the nanoshell and tissue. It causes heat inside the particle to build locally within a short time. The magnitude of the transient temperature difference between the DPL model with phase lagging involved and the classical diffusion model depends on pulsewidth, duty cycle, as well as repetition rate. Within the period of relaxation time of the tissue, larger pulsewidth and high repetition rate result in a larger temperature difference compared to the diffusion results. Keeping the laser power constant, the temperature response of CW-laser irradiation was compared with that of the repetitive pulsed laser. We found that within the framework of the DPL model, the temperature with pulsed laser tends to be lower than the CW results, which is just the opposite in the diffusion model. In addition, under the condition of CW-laser irradiation, we found that the maximal transient temperature is almost as high as 350 times the steady-state temperature. The overheating period is short, but the related biological response could be profound due to the high magnitude of the transient temperature.

#### REFERENCES

- [1] S. Kalele, S. W. Gosavi, J. Urban, and S. K. Kulkarni, "Nanoshell particles: Synthesis, properties and applications," *Curr. Sci.*, vol. 91, no. 8, pp. 1038–1052, 2006.
- [2] V. M. Prida, M. Hernandez-Velez, K. R. Pirota, A. Menendez, and M. Vazquez, "Synthesis and magnetic properties of Ni nanocylinders in self-aligned and randomly disordered grown titania nanotubes," *Nanotechnology*, vol. 16, pp. 2696–2702, 2005.
- [3] B. K. Jena and C. R. Raj, "Shape-controlled synthesis of gold nanoprisms and nanoperiwinkles with pronounced electrocatalytic activity," *J. Phys. Chem.*, vol. 111, pp. 15146–15153, 2007.
- [4] H. S. Zhou, I. Honma, and H. Komiyama, "Controlled synthesis and quantum size effect in gold coated nanoparticles," *Phys. Rev. B*, vol. 50, pp. 12052–12056, 1994.
- [5] J. B. Jackson, S. L. Westcott, L. R. Hirsch, J. L. West, and N. J. Halas, "Surface enhanced Raman effect via the nanoshell geometry," *Appl. Phys. Lett.*, vol. 82, pp. 257–259, 2003.
- [6] C. H. Liu, B. Q. Li, and C. Mi, "Energy absorption of gold nanoshells in hyperthermia therapy," *IEEE Trans. Bionanosci.*, vol. 7, no. 3, pp. 206–214, Sep. 2008.
- [7] R. D. Averitt, S. L. Westcott, and N. J. Halas, "Linear optical properties of gold nanoshells," *J. Opt. Soc. Amer. B*, vol. 16, pp. 1824–1832, 1999.
- [8] R. Weissleder, "A clearer vision for *in vivo* imaging," *Nat. Biotechnol.*, vol. 19, pp. 316–317, 2001.
- [9] P. J. Deren, "Lasers and medicine," *Phys. Status Solidi C*, vol. 1, no. 2, pp. 290–294, 2004.
- [10] T. L. Troy and S. N. Thennadil, "Optical properties of human skin in the near infrared wavelength range of 1000 to 2200 nm," *J. Biomed. Opt.*, vol. 6, no. 2, pp. 167–176, 2001.
- [11] U. Mahmood and R. Weissleder, "Near-infrared optical imaging of proteases in cancer," *Mol. Cancer Ther.*, vol. 2, no. 5, pp. 489–496, 2003.
- [12] H. Jiang, N. V. Iftimia, Y. Xu, J. A. Eggert, L. L. Fajardo, and K. L. Klove, "Near-infrared optical imaging of the breast with model-based reconstruction 1," *Acad. Radiol.*, vol. 9, pp. 186–194, 2002.
- [13] J. L. West and N. J. Halas, "Applications of nanotechnology to biotechnology," *Curr. Opin. Biotechnol.*, vol. 11, pp. 215–217, 2000.
- [14] C. Loo, A. Lin, L. Hirsch, M. H. Lee, J. Barton, N. Halas, J. West, and R. Drezek, "Nanoshell-enabled photonics-based imaging and therapy of cancer," *Technol. Cancer Res. Treat.*, vol. 3, no. 1, pp. 33–40, 2004.
- [15] E. Helm, "Nanotechnology may replace existing treatments for cancer," *Eukaryon*, vol. 3, pp. 55–62, 2007.
- [16] L. R. Hirsch, R. J. Stafford, J. A. Bankson, S. R. Sershen, B. Rivera, R. E. Price, J. D. Hazle, N. J. Halas, and J. L. West, "Nanoshell-mediated near-infrared thermal therapy of tumors under magnetic resonance guidance," *Proc. Nat. Acad. Sci.*, vol. 100, no. 23, pp. 13549–13554, 2003.
- [17] G. G. Akchurin, G. G. Akchurin, and V. A. Bogatyrevb, "Near-infrared laser photothermal therapy and photodynamic inactivation of cells by using gold nanoparticles and dyes," *Proc. SPIE*, pp. 1U-1–1U-12, 2007.
- [18] A. M. Gobin, M. H. Lee, N. J. Halas, W. D. James, R. A. Drezek, and J. L. West, "Near-Infrared resonant nanoshells for combined optical imaging and photothermal cancer therapy," *Nano Lett.*, vol. 7, no. 7, pp. 1929–1934, 2007.
- [19] R. Dua and S. Chakraborty, "A novel modeling and simulation technique of photo-thermal interactions between lasers and living biological tissues undergoing multiple changes in phase," *Comput. Biol. Med.*, vol. 35, pp. 447–462, 2005.
- [20] D. M. Simanovskii, M. A. Mackanos, A. R. Irani, C. E. O'Connell-Rodwell, C. H. Contag, H. A. Schwetman, and D. V. Palanker, "Cellular tolerance to pulsed hyperthermia," *Phys. Rev. E*, vol. 74, pp. 011915–1–011915-7, 2006.
- [21] T. Q. Qiu and C. L. Tien, "Femtosecond laser heating of multi-layered metals—I. Analysis," *Int. J. Heat Mass Transfer*, vol. 37, pp. 2789–2797, 1994.
- [22] T. Q. Qiu, T. Juhacz, C. Suarez, W. E. Born, and C. L. Tien, "Femtosecond laser heating of experiment multi-layered metals-II. Experiment," *Int. J. Heat Mass Transfer*, vol. 37, pp. 2799–2808, 1994.
- [23] D. Y. Tzou, "On the thermal shock wave induced by a moving heat source," *Trans. ASME J. Heat Transfer*, vol. 111, pp. 237–238, 1989.
- [24] A. Majumdar, "Microscale heat conduction in dielectric thin film," *J. Heat Transfer*, vol. 115, pp. 7–16, 1993.
- [25] C. Cattaneo, "A form of heat conduction equation which eliminates the paradox of instantaneous propagation," *Comptes Rendus*, vol. 247, pp. 431–433, 1958.
- [26] P. Vernotte, "Some possible complication in the phenomena of thermal conduction," *Comptes Rendus*, vol. 252, pp. 2190–2191, 1961.
- [27] H. Pan, S. H. Ko, and C. P. Grigoropoulos, "The solid-state neck growth mechanisms in low energy laser sintering of gold nanoparticles—A molecular dynamics simulation study," *J. Heat Transfer*, vol. 130, pp. 092404-1–092404-7, 2008.
- [28] M. I. Kaganov, I. M. Lifshitz, and M. V. Tanatarov, "Relaxation between electrons and crystalline lattices," *Sov. Phys. JETP*, vol. 4, pp. 173–178, 1957.
- [29] S. I. Anisimov, B. L. Kapeliovich, and T. L. Perelman, "Electron emission from Metal surface exposed to ultra-short laser pulses," *Sov. Phys. JETP*, vol. 39, pp. 375–377, 1974.
- [30] T. Q. Qiu and C. L. Tien, "Heat transfer mechanisms during short-pulse laser heating of metals," *ASME J. Heat Transfer*, vol. 115, pp. 835–841, 1993.
- [31] R. A. Guyer and J. A. Krumhansl, "Solution of the linearized Boltzmann equation," *Phys. Rev.*, vol. 148, pp. 766–778, 1966.
- [32] D. Y. Tzou, *Macro-to-Microscale Heat Transfer: The Lagging Behavior*. Washington, DC: Taylor & Francis, 1996.
- [33] B. Q. Li, C. Mi, C. H. Liu, G. Cheng, M. Fu, and G. Meadow, "Nanoparticle heat transfer and its application to laser hyperthermia," *Proc. IMECE'07, ASME Int. Mech. Congr. Expo.*, vol. 11(B), pp. 1093–1100, 2008.
- [34] D. W. Tang and N. Araki, "Wavy, wavelike, diffusive thermal response of finite rigid albs to high-speed heating of laser-pulses," *Int. J. Heat Mass Transfer*, vol. 42, pp. 855–860, 1999.
- [35] T. Okamoto, "Near-field spectral analysis of metallic beads," *Near-Field Optics and Surface Plasmon Polaritons*, vol. 81, New York: Springer-Verlag, 2001, pp. 97–122.
- [36] P. B. Johnson and R. W. Christy, "Optical constants of the noble metals," *Phys. Rev. B*, vol. 6, pp. 4370–4379, 1972.
- [37] D. Y. Tzou and J. K. Chen, "Thermal lagging in random media," *J. Thermophys. Heat Transfer*, vol. 12, pp. 567–574, 1998.

- [38] A. Vedavarz, S. Kumar, and M. K. Moallemi, "Significance of non-Fourier heat waves in conduction," *J. Heat Transfer*, vol. 116, pp. 221–223, 1994.
- [39] K. Mitra, S. Kumar, A. Vedavarz, and M. K. Moallemi, "Experimental evidence of hyperbolic heat conduction in processed meat," *ASME J. Heat Transfer*, vol. 117, pp. 568–573, 1995.
- [40] W. Kaminski, "Hyperbolic heat conduction equation for materials with a nonhomogeneous inner structure," *ASME J. Heat Transfer*, vol. 112, no. 3, pp. 555–560, 1990.
- [41] A. Banerjee, A. A. Ogale, C. Das, K. Mitra, and C. Subramanian, "Temperature distribution in different materials due to short pulse laser irradiation," *Heat Transfer Eng.*, vol. 26, no. 8, pp. 41–49, 2005.
- [42] M. Hu and G. V. Hartland, "Heat dissipation for Au particles in aqueous solution: Relaxation time versus size," *J. Phys. Chem. B*, vol. 106, pp. 7029–7033, 2002.
- [43] A. Plech, V. Kotaidis, S. Grésillon, C. Dahmen, and G. V. Plessen, "Laser-induced heating and melting of gold nanoparticles studied by time-resolved x-ray scattering," *Phys. Rev. B*, vol. 70, pp. 195423-1–195423-7, 2004.
- [44] A. Plech, V. Kotaidis, M. Lorenc, and M. Wuff, "Thermal dynamics in laser excited metal nanoparticles," *Chem. Phys. Lett.*, vol. 401, pp. 565–569, 2005.



**Ben Q. Li** received the B.S. degree from Central University, Hunan, China, in 1982, the M.S. degree from Colorado School of Mines, Golden, in 1984, and the Ph.D. degree from the University of California, Berkeley, in 1989, all in mechanical engineering.

He was a Research Associate at Massachusetts Institute of Technology for about a year, and a Senior Engineer at Aluminum Company of America (Alcoa) for three years before joining academia in 1994. He is currently a Professor and Chair of the Department of Mechanical Engineering, University of Michigan Dearborn, Dearborn. He is the author of a book and over 200 published articles and the editor of two books. He has been the invited keynote speaker at many domestic and international conferences and his research work has been supported by various federal (National Science Foundation, National Aeronautics and Space Administration, Department of Energy, Department of Defense, National Institute of Standards and Technology) and state agencies as well as private industries. His current research interests include the study of electromagnetics, fluid flow, and heat transfer in thermal-fluid systems.

Prof. Li is a Fellow of the American Society for Mechanical Engineers.



**Changhong Liu** received the B.S. degree in electrical engineering from Hefei University of Technology, Hefei, China, in 1992, the M.S. degree from Tsinghua University, Beijing, China, in 2001, and the Ph.D. degree from Shanghai Jiao Tong University, Shanghai, China, in 2009.

Since 2001, she has been a Lecturer at Shanghai Jiao Tong University. She is currently a Postdoctoral Fellow at the University of Michigan Dearborn, Dearborn. Her current research interests include electromagnetic field, heat transfer, and cooling

technology.



**Chunting Chris Mi** (S'00–A'01–M'01–SM'03) received the B.S.E.E. and M.S.E.E. degrees from Northwestern Polytechnical University, Xi'an, China, and the Ph.D. degree from the University of Toronto, Toronto, ON, Canada, all in electrical engineering.

He was initially with the Rare-Earth Permanent Magnet Machine Institute, Northwestern Polytechnical University. He joined the Xi'an Petroleum Institute as an Associate Professor and Associate Chair of the Department of Automation in 1994. He was a Visiting Scientist at the University of Toronto from 1996 to 1997. From 2000 to 2001, he was an Electrical Engineer with General Electric Canada, Inc. He was responsible for designing and developing large electric motors and generators up to 30 MW. He is currently an Associate Professor and Director of DTE Power Electronics and Electrical Drives Laboratory at the University of Michigan Dearborn, Dearborn. He has conducted extensive research and is the author or coauthor of more than 80 published articles on the subject of electric machines, power electronics, and electric and hybrid vehicles. His current research interests include electric drives, power electronics, electric machines, renewable energy systems, and electric and hybrid vehicles.

Dr. Mi is the Chair of the IEEE Southeastern Michigan section (2008–2009). He was the Vice Chair of the Section from 2006 to 2007. He is the recipient of the "National Innovation Award," "Government Special Allowance Award," "Distinguished Teaching Award," and "Distinguished Research Award" of the University of Michigan Dearborn. He is also a recipient of the 2007 IEEE Region 4 "Outstanding Engineer Award," "IEEE Southeastern Michigan Section Outstanding Professional Award," and the "SAE Environmental Excellence in Transportation (E2T) Award."